Nanoscale

Accepted Manuscript

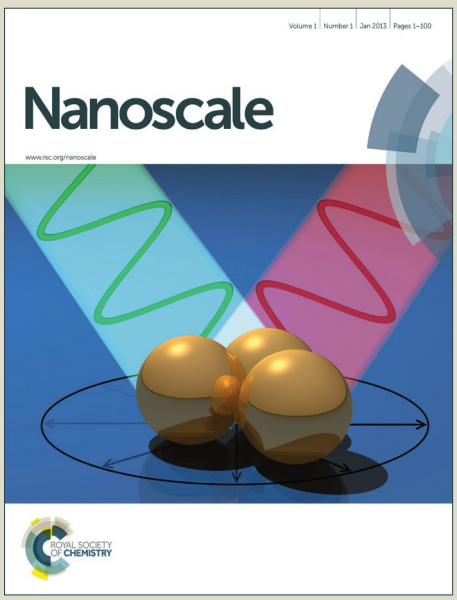

ROYAL SOCIETY OF CHEMISTRY

www.rsc.org/nanoscale

The SPL7013 Dendrimer Destabilizes the HIV-1 gp120-CD4 Complex

Bidisha Nandy[1,2,+], Suman Saurabh[1,+], Anil Kumar Sahoo[1], Narendra M. Dixit[3,4,*] and Prabal K. Maiti[1,*]

[1]Center for Condensed Matter Theory, Department of Physics, Indian Institute of Science, Bangalore

[2]Department of Physics, Lovely Professional University, Punjab

[3]Department of Chemical Engineering, and [4]Centre for Biosystems Science and Engineering, Indian Institute of Science, Bangalore

[+]Equal contribution

[*]Correspondence: narendra@chemeng.iisc.ernet.in; maiti@physics.iisc.ernet.in

ABSTRACT

The poly (l-lysine)-based SPL7013 dendrimer with naphthalene disulphonate surface groups blocks the entry of HIV-1 into target cells and is in clinical trials for development as a topical microbicide. Its mechanism of action against R5 HIV-1, the HIV-1 variant implicated in transmission across individuals, remains poorly understood. Using docking and fully atomistic MD simulations, we find that SPL7013 binds tightly to R5 gp120 in the gp120-CD4 complex but weakly to gp120 alone. Further, the binding, although to multiple regions of gp120, does not occlude the CD4 binding site on gp120, suggesting that SPL7013 does not prevent the binding of R5 gp120 to CD4. Using MD simulations to compute binding energies of several docked structures, we find that SPL7013 binding to gp120 significantly weakens the gp120-CD4 complex. Finally, we use steered molecular dynamics (SMD) to study the kinetics of the dissociation of the gp120-CD4 complex in the absence of the dendrimer and with the dendrimer bound in each of the several stable configurations to gp120. We find that SPL7013 significantly lowers the force required to rupture the gp120-CD4 complex and accelerates its dissociation. Taken together, our findings suggest that SPL7013 compromises the stability of the R5 gp120-CD4 complex, potentially preventing the accrual of the requisite number of gp120-CD4 complexes across the virus-cell interface and thereby blocking virus entry.

I. Introduction

The dendrimer SPL7013 is the active ingredient in the topical microbicide formulation VivaGel, currently in clinical development for the prevention of the sexual transmission of HIV-1[1-4]. Given the lack of vaccines and successful treatment options for HIV-1 infection, topical microbicides that can prevent transmission present a promising alternative to control the HIV epidemic, especially in settings where women are not empowered to abstain or enforce condom usage. SPL7013 displayed potent activity in vitro against diverse HIV-1 strains[5, 6], was successful in preventing transmission in animal models[7], and has been found safe for once daily application in healthy women for up to a week[8] . It also displayed activity against herpes simplex virus (HSV)[6, 7] and is in clinical development for the prevention and treatment of bacterial vaginosis[9].

Several studies have focused on elucidating the mechanism of action of SPL7013 against HIV-1 (e.g.,(3,5); reviewed in (3)). Based on in vitro time-of-addition experiments, SPL7013 is thought to prevent viral entry into target cells[6]. HIV entry requires the binding of the viral envelope proteins gp120 to cell surface receptors CD4 and, subsequently, co-receptors, either CCR5 or CXCR4[10]. Virions that require CCR5 for entry are termed R5 virions, those that require CXCR4 are termed X4 virions, and those that can use either are termed R5X4 virions. SPL7013 appears to block the entry of these diverse strains in different ways: In one set of experiments, target cells in the presence of SPL7013 were exposed to virions and the efficacy of SPL7013 in blocking infection assessed. In these experiments, SPL7013 prevented infection by both R5 and X4 virions with comparable efficacies[6]. In another set of experiments, virions were first exposed to SPL7013 and then employed to infect target cells in the absence of SPL7013. In the latter experiments, the infectivity of X4 and R5X4 virions was compromised to an extent similar to that when SPL7013 was present in culture[11]. Further, SPL7013 did not degrade HIV or reduce gp120 expression[11]. Thus, SPL7013 appears to bind X4 HIV-1 gp120 and block its binding to CD4 and/or CXCR4, thereby preventing virus entry. In contrast, the infectivity of SPL7013-exposed R5 virions was much higher than when SPL7013 was present in culture[11]. The binding of SPL7013 to R5 gp120 may thus be much weaker than to X4 gp120. How SPL7013 blocks the entry of R5 HIV-1 when present in culture thus remains unknown. Given that viral strains involved in transmission are predominantly R5[12], understanding the mode of action of SPL7013 against R5 HIV-1 may be important in deducing guidelines for its optimal usage.

We hypothesized that SPL7013 could bind to the R5 gp120-CD4 complex and destabilize it. Indeed, SPL7013 has been suggested to bind to regions on gp120 exposed following conformational changes induced upon CD4 binding[6]. Multiple gp120-CD4-CCR5 complexes are thought to be required

for virus entry[13, 14]. By destabilizing the gp120-CD4 complex, SPL7013 may not allow the formation of the requisite number of receptor complexes and thus prevent entry. To test our hypothesis, we employed molecular docking to determine the ability of SPL7013 to bind gp120 alone or in complex with CD4. We then employed fully atomistic molecular dynamics simulations to evaluate the energetics and the kinetics of dissociation of the gp120-CD4 complex in the presence and absence of the SPL7013 dendrimer. We find that SPL7013 docks to gp120 in the R5 gp120-CD4 complex but not to R5 gp120 alone, weakens the gp120-CD4 complex and accelerates its dissociation. Our study thus elucidates a potential mechanism of the action of SPL7013 against R5 HIV-1, informing future strategies that might use SPL7013 for blocking the transmission of HIV-1.

II. Methods

Modeling the SPL7013 dendrimer

We built the structure of the SPL7013 dendrimer using our in-house Dendrimer Builder Toolkit (DBT)[15]. The core, repeating unit, and terminal residue employed (Fig. 1) were designed as per the chemistry and topology of the dendrimer[6]. Residues with cap(s) were optimized individually using GAUSSIAN03[16] with the HF/6-31+G (d,p) basis set. Using Antechamber[17], charges were provided with the restrained electrostatic potential (RESP) fitting method implemented in AMBER. Charge for the atoms forming the caps was constrained to zero. The overall charge on the core and repeating residues (Fig. 1) was also set to zero, whereas the charge on the terminal de-protonated residue was set to -2 (representing two de-protonated carboxyl groups). Finally, caps from residues were removed using the *xleap* module in AMBER and the de-capped residues thus obtained were used for building the dendrimer using DBT. GAFF atom types along with RESP charges for the de-capped residues are provided in Table S1 of the Supplementary Information (SI). In the resulting dendrimer structure, the linear chains of the repeating fragment were found to cross-sect the terminal rings at a few places. The few such entanglements were removed manually with local relaxation using the *xleap* module in AMBER. The generation 4 (G4) SPL7013 dendrimer thus obtained is shown in (Fig. 1).

MD simulation of the dendrimer

We used the AMBER12 software package[18] with GAFF set of parameters for the SPL7013 G4 dendrimer. The dendrimer was solvated by a 13Å hydration cell using the TIP3P model for water[19] using the *leap* module of AMBER12 tools. To neutralize the anionic dendrimer, we added 64 Na+ ions in the system. The solvated structure was subjected to 1000 steps of steepest descent minimization followed by 2000 steps of conjugate gradient minimization, during which process the dendrimer was

restricted to its initial conformation using harmonic constraints with a force constant of 500 kcal/mol/Å^2 and the water molecules were allowed to reorganize and eliminate unfavorable contacts with the dendrimer. The system was further subjected to 5000 steps of conjugate gradient minimization, with the harmonic constraints on the solute relaxed from 20 kcal/mol/Å^2 to 0 with a reduction of 5 kcal/mol/Å^2 every 1000 steps. Then 40 ps of MD simulation with a 2 fs time step for integration was performed to get an energy-minimized structure. During the MD simulation, the system was gradually heated from 0 to 300 K using weak 20 kcal/mol/Å^2 harmonic constraints on the solute to its starting structure, which allowed slow relaxation of the dendrimer. NVT dynamics was employed using the SHAKE method[20] with a geometrical tolerance of $5x10^{-4}$ Å on all covalent bonds involving hydrogen atoms. The Particle Mesh Ewald (PME) method was used for long range electrostatic interactions with a real space cut-off of 9 Å. Finally, the system was subjected to 2 ns of NVT simulation, which was followed by 82 ns of NPT simulation. All simulations were carried out using PMEMD module[21] of AMBER12. A similar simulation protocol was followed in our earlier work to achieve stable equilibrated dendrimer structures[22, 23]. The resulting structure was employed for docking and subsequent simulations.

MD simulation of gp120 and the gp120-CD4 complex

We used the crystal structure of the YU2 gp120 core complexed with CD4 and a functionally sulfated antibody F12d (PDB: 2QAD)[24], from which we removed the antibody and subjected the resulting gp120-CD4 complex to solvation and energy minimization as described above. The system contained 275726 atoms with 89310 water molecules and 9 Cl^- ions. We then carried out a 100 ns long MD simulation using the NVT ensemble.

Simultaneously, from the above crystal structure, we removed both CD4 and the F12d antibody and obtained the structure of monomeric gp120. The structure was solvated in TIP3P water with a 30 Å buffer and then neutralized by 5 Cl^- ions using the *xleap* module of AMBER12. ff99SB[25] was used to describe inter and intramolecular interactions involving gp120-CD4. The structure was minimized and equilibrated in the NPT ensemble and then a further 100 ns of NVT run was carried out.

The resulting structures of gp120 and the gp120-CD4 complex were employed for docking and simulation studies.

Docking of SLP7013 to gp120 and to the gp120-CD4 complex

We used ZDOCK[26], an automated protein docking server, for docking the gp120-CD4 complex and the de-protonated SPL7013 dendrimer. The gp120-CD4 complex after 40 ns of MD simulation in an NVT ensemble and the dendrimer after 80 ns of MD simulation in an NPT ensemble (see above)

were employed as the receptor and the ligand, respectively, for docking. (We also employed several other structures of the dendrimer between 70 and 80 ns of MD simulation to examine the robustness of our findings to the initial structures employed; please see below.) The input parameters were kept at their default values in ZDOCK. Of the resulting docked structures, we considered the top 8 (Fig. 2) for further analysis. We repeated the above procedure with gp120 alone (using a structure after 50 ns of MD simulation) as receptor and found that two of the top 10 docked structures predicted (ranks 1 and 8) had SPL7013 bind near the V3 loop of gp120. We selected these structures for further studies (see below).

MD simulation and energetics of docked structures

Even though ZDOCK assigns ranks based on sophisticated scoring functions, a calculation of binding energy is necessary in light of the CAPRI test runs[27], where ZDOCK predicted correct binding poses for only half of the targets used in the study. Accordingly, we performed MD simulations of the docked structures chosen above to compute their binding energies and examine their stability.

Each of the docked structures above was immersed in a water box (with at least a 30Å water layer in all the three directions). 64 Na^+ ions and 9 Cl^- ions were added for charge neutrality. Details of the resulting system sizes are in Table S2 of the SI. The structures were allowed to equilibrate (see above) and subjected to 60 ns or more of MD simulation in an NVT ensemble. The binding energy between gp120-CD4 (receptor) and the dendrimer (ligand) was then calculated using the MMPBSA[28] module of AMBER12. Entropy calculations were also performed using MMPBSA and normal mode analysis (see below). From the binding energy calculations, we found that the highest ranked ZDOCK structure was not the most stable. We chose the top 4 stable structures based on our energy calculations (ZDOCK ranks 6, 8, 3, and 2, respectively) for further analysis. As a control, we also included the least stable structure (ZDOCK rank 4). The latter complexes were simulated further, up to 100 ns, to ensure their stability.

In the latter structures, SPL7013 bound near the V3 loop of gp120, in accordance with earlier suggestions[6]. Accordingly, for our studies of SPL7013 binding to gp120 alone, we chose docked structures where the binding was near the V3 loop (see above). We followed the same protocol of MD simulations described above to get well equilibrated complexes and then computed their binding energies.

Steered molecular dynamics (SMD) simulations

SMD simulations were performed by pulling an atom near the center-of-mass (COM) of CD4 while keeping the COM of gp120 fixed. During the equilibrium simulations above, the gp120-CD4

complexes, both in the presence and the absence of dendrimer, underwent significant tilting, as a result of which the complexes initially aligned along the length ended up aligned along a shorter edge of the simulation box. We therefore selected an initial configuration for the SMD simulations from among the equilibrated snapshots such that the complex was not so heavily tilted that it interacted with its periodic image during pulling. Force was applied to the pulled atom via a harmonic restraint (k = 5 kcal/mol/Å^2) in the direction of the line joining the two COMs $\vec{n}$, such that the atom being pulled moved with a constant velocity v[29]. The effective SMD potential is given by $U(\vec{r}) = \frac{k}{2}[vt - (\vec{r} - \vec{r}_0).\vec{n}]^2$, and the resulting pulling force, $\vec{F} = -\nabla U$, where k is the force constant, and $\vec{r}$ and $\vec{r_0}$ are the positions of the COM of the protein being pulled at time t and at the initial time, respectively. SMD simulations were performed using the software package NAMD[30].

Calculation of binding energy and entropy of the gp120-CD4 complex

We used the MM-PB/GB-SA method[31] (MM: Molecular Mechanics; PB: Poisson-Boltzmann; GB: Generalized Born; SA: Surface Area) employed in the MMPBSA.py[28] module of AMBER12 to calculate the binding energy of the gp120-CD4 complex: $\Delta G_{bind} = G_{complex} - G_{gp120} - G_{CD4}$. The binding energy is computed as $\Delta G_{bind} = \Delta E_{bind} - T\Delta S_{bind}$, where $\Delta E_{bind} = \Delta E_{ele} + \Delta E_{vdw} + \Delta E_{\text{int}} + \Delta E_{sol}$ is the sum of the changes in the electrostatic energy, ΔE_{ele}, non-bond van der Waals energy, ΔE_{vdw}, the internal energy from bonds, angles and torsions, ΔE_{int}, and the contribution from the solvent, ΔE_{sol}. The latter contribution, $\Delta E_{sol} = \Delta E_{es} + \Delta E_{nes}$, is the sum of the electrostatic energy, ΔE_{es}, calculated using the Poisson-Boltzmann (PB) method, and the non-electrostatic energy, ΔE_{nes}, calculated as $\gamma SASA + \beta$, where γ = 0.00542 kcal/Å^2 is the surface tension, β = 0.92 kcal/mol, and $SASA$ is the solvent-accessible surface area of the molecule[32]. The time series of the binding free energy of the gp120-CD4 complex was determined using gas-phase energies (MM) and solvation free energies following the Generalized Born model (GB/SA) analysis from snapshots obtained from a total of 100 ns of MD simulation. We performed similar calculations to estimate the binding energies of SPL7013 to gp120 alone or in complex with CD4.

Entropy calculations were performed for the gp120-CD4 complex alone or bound to SPL7013 again using MMPBSA.py[28]. The latter module calculates rotational and translational entropies assuming a rigid rotor model. To calculate the vibrational entropies, we employed normal mode analysis. First, minimization was performed so that the system relaxed to the nearest local minimum

and then vibrational frequencies were calculated through the diagonalization of the Hessian matrix. As the calculation is computationally intensive for the system sizes we deal with here, we calculated the entropy averaged over 10 frames extracted from the well equilibrated regions of the MD trajectories.

Calculation of the number of contacts and analysis of the interface between molecules

We used the following criteria to calculate the number of intermolecular contacts. When an atom of CD4 fell within 3 Å of any atom in gp120, the two atoms were considered a contact between the two molecules. This contact analysis identified each atom of gp120 and CD4 responsible for making contacts between the two molecules. We identified the residues that resulted in contacts with and without the bound dendrimer.

To analyse the gp120-dendrimer interface, we calculated the residue-wise energetic contribution to the total binding energy using the MMPBSA module of AMBER12. To select the residues involved, we performed contact analysis as described above. We selected all the residues of gp120 that were within 3Å of the dendrimer and calculated the energy contributions for those residues. The contribution of each residue to the different energy components (van der Waals, electrostatic, polar solvation and non-polar solvation) was summed to obtain the relative contributions of the different energy components to the total binding energy, giving insights into the nature of the interaction between the dendrimer and gp120.

III. Results

SPL7013 docked to gp120 in the gp120-CD4 complex

We modeled the generation 4 (G4) SPL7013 dendrimer using our Dendrimer Building Toolkit (DBT), solvated it and equilibrated the solvated structure using MD simulations (Methods). The structure became stable after ~50 ns of equilibration (Fig. 1). The resulting structure had a similar radius of gyration (R_g) to that obtained by previous MD simulations[33], giving us confidence in our model of the SPL7013 dendrimer. The RMSD of the dendrimer along its MD trajectory also indicates a stable structure, although some fluctuations due to the highly mobile terminal groups were always present (Fig.1). Similarly, we also obtained equilibrated structures of gp120 and the gp120-CD4 complex, both derived from the crystal structure of the gp120-CD4 complex in the presence of an antibody (Methods).

We next docked the equilibrated dendrimer to the equilibrated gp120-CD4 complex using ZDOCK. We recognize that the top ranked docked structure predicted by ZDOCK need not be energetically the most stable[27]. We therefore considered the top 8 docked structures predicted by

ZDOCK for further analysis (Fig. 2). The structures indicate the diversity of the potential binding conformations of the dendrimer to the gp120-CD4 complex. In all cases, though, the dendrimer bound to gp120 in the gp120-CD4 complex, in agreement with earlier findings[6]; binding to CD4 was not observed. To assess the stability of the latter structures, we solvated each structure and performed MD simulations in the absence of any external force (Methods). The RMSDs of the complexes converged rapidly, in ~20-30 ns (Figs. 3, S1 and S2). We subjected each structure to 60-100 ns long simulation, which was adequate for us to compute equilibrium properties accurately.

We calculated the binding energy and entropy of SPL7013 to gp120 in the gp120-CD4 complex from the MD simulations above (Table 1). The ranking of the structures predicted by ZDOCK did not match the rankings based on our energy calculations. This may not be surprising as in the CAPRI test runs[27] ZDOCK predicted correct binding poses for only half of the targets used. Thus, we considered the rank ordering based on our free energy calculations for the choice of structures for further analysis. The top 4 structures had significantly favorable ΔG values (-71±20 kcal/mol for the first to -49±17 kcal/mol for the fourth), indicating tight binding of the dendrimer to the gp120-CD4 complex (the corresponding ΔE values ranged from -182±10 kcal/mol to -146±9 kcal/mol). The remaining structures did not appear to have significantly favorable ΔG values (-29±16 kcal/mol for the fifth and -4±29 for the last), indicating weak binding. We therefore chose the first 4 (most stable) structures and, as a control, the last (least stable) structure, for further analysis. In the rest of the text we refer to a complex by its rank with respect to the binding free energy (ΔG). The rankings are listed in Table 1.

A decomposition of the binding energy into its constituent parts revealed that the electrostatic part provides the most dominant stabilizing contribution to the total binding energy. (The breakup of the total binding energy into its constituent terms for complexes 1 and 3 are listed in Table S3.) Polar solvation is the most unfavorable, due to the shielding of polar residues from water on dendrimer binding. Non-polar solvation also has a stabilizing contribution due to the hydrophobic stabilization of the aromatic rings of the dendrimer. The aromatic rings were observed to form stacked structures with LYS, ARG, ASN and PRO residues of gp120 (Fig. S3). Such stacking interactions between aromatic rings and charged residues like ARG are well documented in the literature [34, 35]. The electrostatic potential map of gp120-CD4 surface shows that the V3 loop is a region of high positive electrostatic potential contributing significantly to the total energy (Fig. S4).

To further verify the large binding energies that we obtain from MMPBSA, we performed an MD simulation with the dendrimer placed away from gp120-CD4 complex. We observed that the dendrimer very quickly attached itself to gp120 near the V3 loop (Fig. S5). To check the effect of

dendrimer conformation, which may vary significantly even when the R_g has converged, on the binding energy, we performed docking with four other dendrimer structures corresponding to 68ns, 72ns, 76ns and 78ns of the MD trajectory of the free dendrimer. We observed that the preferred docking positions were similar for all the four structures (Table S4). We simulated the structures (one for each initial dendrimer conformation) where the dendrimer bound near the V3 loop of gp120 for 50 ns and calculated the gp120-dendrimer binding energy. We obtained an average binding energy of -152 kcal/mol, which is close to the value of -166 kcal/mol for the four complexes with the 80 ns dendrimer structure docked near the V3 loop that are discussed above. Details of the binding energies are in Table S5.

SPL7013 docked weakly to gp120 alone

To check whether SPL7013 could bind to gp120 alone, we next docked the equilibrated dendrimer to the equilibrated structure of gp120. We again considered the top 8 structures predicted by ZDOCK and found among them that the first and eighth ranked structures had the dendrimer bind on/near the V3 loop of gp120 (Fig. 4). During our simulations of the gp120-CD4-SPL7013 complexes above, we found that for structures where the dendrimer docked away from the V3 loop, the dendrimer exhibited large amplitude motion towards the loop (Fig. S6), suggesting that the V3 loop region is a low energy region for dendrimer binding, probably owing to the high positive charge density in this region. We therefore chose the two gp120-SPL7013 structures where the dendrimer bound near the V3 loop for further analysis. Solvation and MD simulations suggested that the docked structures remained stable (Fig. 4). The dendrimer binding to gp120, however, was much weaker than in the ternary complex. The mean ΔE for the latter two structures was -99±10 kcal/mol, in contrast to the mean of -166±10 kcal/mol in the top 4 ternary complexes (Table 1) (the mean for all the eight structures is -136±10 kcal/mol).

CD4 binding to gp120 is known to induce conformational changes in gp120 crucial to the neutralization of the virus by various antibodies that bind to the V3 loop; antibodies recognize CD4 bound gp120 whereas they do not bind to gp120 alone[36]. When soluble CD4 binds to HIV-1 gp120, the variable loops, V1/V2 and V3, undergo conformational changes and become more exposed[36-39]. In accordance with these experimental observations, we found conformational differences in gp120 in the presence and absence of bound CD4. Using the electrostatic potential surface of gp120, a conserved region near the base of the V3 loop was identified as a possible dendrimer binding site[6]. We also observed significant differences in the V3 base as well as the bridging sheet region due to CD4 binding

(Fig. S7). A key part of the gp120-dendrimer binding energy in presence of CD4 comes from the long range electrostatic component. We therefore calculated the binding energy including and excluding the contribution from CD4. For complex 1, the gp120-dendrimer binding energy was -182±10 kcal/mol, while when we excluded the effect of CD4, the energy turned out to be -159±13 kcal/mol. This reduction stems from the electrostatic contribution of CD4 to the gp120-dendrimer binding. Thus, conformational changes in the V3 loop and bridging sheet region of gp120 as well as the increased electrostatic interaction resulted in tighter binding of the dendrimer to gp120 in the presence of bound CD4.

We also examined whether the dendrimer could bind to the CD4 binding region of gp120 and thus prevent the formation of the gp120-CD4 complex. ZDOCK did not yield any structures where the dendrimer docked to the CD4 binding region on gp120, while the docking software Patchdock yielded as its tenth ranked structure a complex where the dendrimer docked to gp120 such that it blocked its CD4 binding region (Fig. 4). We performed MD simulations with this latter structure and found its binding energy to be -41±25 kcal/mol, which is much lower than that for structures where the dendrimer docks near the V3 loop of gp120.

We concluded thus that SPL7013 bound strongly to gp120 in the gp120-CD4 complex and not to gp120 alone. The dendrimer also did not appear to block the CD4 binding site of gp120 effectively. We examined next how SPL7013 affected the gp120-CD4 complex.

SPL7013 weakened the gp120-CD4 complex

We examined the gp120-CD4 complex with and without the docked SPL7013 and found that SPL7013 altered the conformation of the gp120-CD4 complex and weakened it. In the absence of the dendrimer, the binding energy of the gp120-CD4 complex was -67±7 kcal/mol, consistent with experiments[40] and with our previous simulations[22]. We also calculated the entropy of the complex and found an entropic contribution of 54±6 kcal/mol to the binding free energy. The binding energy and entropy obtained from our simulations are close to experimental values (ΔE = -62±3 kcal/mol and $T\Delta S$ = 53±3 kcal/mol)[40]. SPL7013 reduced the binding energy of the gp120-CD4 complex. The binding energy of gp120 and CD4 in the top 4 equilibrated ternary complex structures (see above) was on average significantly lower than that of the binary gp120-CD4 complex (Figs. 3 and S8). The energies ranged from -40±7 to -68±7 kcal/mol for the structures with a mean of -56±7 kcal/mol (Table 2). Surprisingly, the least stable ternary complex also showed significant lowering of the binding energy to -47±8 kcal/mol.

The number of contacts between gp120 and CD4 also showed a reduction upon dendrimer binding (Figs. 3 and S8). On closer examination of the structures, we identified 37 residues in gp120 that were involved in contacts between gp120 and CD4. We found that dendrimer binding typically reduced the number of contacts at several of these residues (Fig. 5). For instance, the number of contacts for residues TRP-254 and ASP-284 were significantly reduced upon dendrimer binding in all the five ternary complex structures. Similarly, several residues that formed contacts in the absence of the dendrimer lost all their contacts upon dendrimer binding. At the same time, although fewer, there were some contacts in the ternary complexes that were absent in the binary complex. These conformational changes are attributable to the positive charge on gp120, especially its V3 loop, which attracts the negatively charged SPL7013, resulting in the destabilization of the gp120-CD4 complex.

SPL7013 facilitated the dissociation of the gp120-CD4 complex

A consequence of the destabilization would be easier dissociation of the gp120-CD4 complex in the presence of SPL7013. To test this, we performed SMD simulations of the selected ternary complexes, where the dissociation of the complex is orchestrated by an external force (Methods). We modulated the force to ensure a constant velocity of separation, ν, between the centers of mass (COMs) of gp120 and CD4. We repeated the simulations for a wide range of values of ν, 0.16 Å/ps to 0.0021 Å/ps, and in each case recorded the instantaneous applied force and the separation between the COMs of gp120 and CD4. For obtaining statistically significant results, we performed three pulling runs at each value of ν for each complex.

At any velocity ν, the external force initially increased with separation. The complex thus resisted stretching due to the applied force. Beyond a certain separation, the force began to decrease, signifying bond dissociation, and eventually vanished (Fig. 6 and Figs. S9-S14). SPL7013 tended to lower the maximum force applied, termed the rupture force, *F*, as well as the separation at which the applied force vanished (Fig. 6). SPL7013 thus enabled dissociation of the gp120-CD4 complex at a lower external force and also triggered complete dissociation over a smaller separation between the COMs of gp120 and CD4. The latter findings are in keeping with the weakening of the gp120-CD4 complex by SPL7013 observed above. Complete dissociation over shorter intermolecular separations is consistent with the fewer contacts between the molecules in the presence of SPL7013 which may therefore be broken more readily freeing the molecules of each other's influence. SPL7013 induced different extents of reduction in *F* in the different ternary complexes (Figs. 6 and S15), indicating the importance of the binding location. On average, however, the reduction in *F* was significant (Fig. 6),

indicating a marked acceleration of the dissociation of the gp120-CD4 complex due to the dendrimer.

This destabilization of the gp120-CD4 complex was due to the conformational changes in gp120 induced by the dendrimer. With complex 3, for instance, the dendrimer, which hangs onto the V3 loop (Fig. 2) caused a significant tilt in gp120 with respect to CD4 (Fig. 7). A comparison between the residue-wise contacts (Fig. 5) showed that the gp120 residues that show a reduction in the number of contacts with CD4 upon dendrimer binding belonged to the regions 1 and 2 of the interface in Fig. 7. These residues belong to the rear part of gp120 (region 1) and the bridging sheet (region 2). The reduction in the number of contacts in region 1 can be understood from the tilt in gp120 induced by the dendrimer. Due to the tilting, the residues move away from CD4 and hence cannot form atomic contacts with it. We also observed that the aromatic rings of the dendrimer interacted electrostatically with LYS-259 and some other residues of the beta sheet, hence stretching the beta sheet farther away from PHE-362 of CD4, resulting in a reduction of contacts between ASN-252 and TRP-254 of gp120 (both belong to the bridging sheet and form large number of contacts with PHE-362 in the absence of dendrimer) and CD4. This in turn contributed to the reduction in the number of contacts between gp120 and CD4. One can observe the difference in the conformation of the bridging sheet due to dendrimer binding (region 2 in Fig. 7(A)). Snapshots indicating the reduction in the number of hydrogen bonds between the above residues of gp120 and CD4 upon dendrimer binding as well as the interaction of the aromatic groups of the dendrimer with the gp120 residues belonging to the bridging sheet giving rise to conformational changes in the sheet are shown in Fig. 8. Finally, we note that in earlier MD studies it has been established that the charge of the V3 loop, which acts as an electrostatic modulator of the gp120 interaction surface, considerably affects the CD4 binding affinity of gp120 through conformational changes in its CD4 binding loop[41]. Binding of the negatively charged dendrimer to the V3 loop may influence these conformational changes and alter the effective charge of the V3 loop seen by rest of the protein, compromising the stability of the gp120-CD4 complex.

In summary, SPL7013 bound to R5 gp120 in the gp120-CD4 complex, weakened the complex and facilitated its dissociation, potentially underlying its ability to prevent HIV-1 entry into target cells.

IV. Discussion

The dendrimer SPL7013, in clinical trials as the topical microbicide formulation VivaGel, prevents HIV-1 entry into target cells. While its virucidal activity may explain its antiviral activity against X4 and R5X4 virions[11], its mechanism of action against R5 virions remains poorly understood. Here, using molecular docking along with fully atomistic molecular dynamics and steered molecular

dynamics simulations, we predict that SPL7013 docks strongly to R5 gp120 in the gp120-CD4 complex but not gp120 alone, weakens the gp120-CD4 complex and facilitates its dissociation. Consequently, adequate gp120-CD4-CCR5 complexes may not form across a virus-cell pair, preventing viral entry. Our study thus presents a potential mechanism by which SPL7013 blocks the entry of R5 HIV-1 into target cells.

In a recent study, we identified that the gp120-CD4 complex dissociated via complex pathways in response to an external force[22] and that the polyamidoamine (PAMAM) dendrimer docked to gp120 in the complex and destabilized the complex. Here, we found similarly that SPL7013 docked to gp120 in the complex and destabilized it. We speculate therefore that other polyanionic dendrimers may also act against HIV-1 by destabilizing the gp120-CD4 complex.

Because our simulations provide atomistic resolution, we were able to identify contact residues between gp120 and CD4 that were altered by the binding of SPL7013 to gp120. Several of the residues lost all their contacts upon dendrimer binding. Some of these losses were due to conformational changes in gp120 induced by SPL7013, which we identified. SPL7013 thus weakened the complex by lowering the net intermolecular contacts between gp120 and CD4. We speculate that the residues displaying differential binding may be involved in the potential development of resistance to SPL7013. The highly branched and open structure of dendrimers typically results in multivalent binding of the dendrimers to their targets. SPL7013 too binds at multiple sites to gp120. Abrogating this binding may thus require gp120 to acquire mutations at these multiple sites. On the other hand, if gp120 could mutate at some of its residues involved in differential binding to CD4, it may retain sufficiently tight binding to CD4 even in the presence of SPL7013. A similar mechanism of resistance is observed with the allosteric inhibitor of gp120-CCR5 binding, maraviroc, where gp120 mutations facilitate CCR5 binding even when maraviroc is bound to gp120[42].

The equilibrium energy and entropy of binding of the gp120-CD4 complex we calculated were in close agreement with experiments. Our SMD simulations, however, could not be compared directly with experiments. Although we employed a wide range of pulling velocities, the velocities were several orders of magnitude larger than those in experimental single molecule force spectroscopy of the HIV-1 gp120-CD4 complex[43]. The large velocities were employed for computational feasibility. In a previous study[22], our SMD simulations have captured qualitative features of the dissociation of the gp120-CD4 complex observed experimentally, giving us confidence in our modeling and simulations. Translating our findings into guidelines for the optimal usage of SPL7013 requires, additionally, knowledge of the minimum number of gp120-CD4-CCR5 complexes across a virus-cell pair for entry, a quantity that

continues to remain elusive[13, 14]. SPL7013 would have to destabilize gp120-CD4 complexes enough to prevent the formation of the latter number of complexes. Integrating our findings of the extent of destabilization of individual gp120-CD4 bonds by SPL7013 with more coarse-grained models of the interactions of gp120, CD4 and CCR5 across a virus-cell synapse may prove a fruitful extension of our work towards the rational identification of guidelines for the optimal usage of SPL7013.

Acknowledgment

This work was funded by the DST Mathematical Biology Initiative at the Indian Institute of Science, Bangalore and by a Wellcome Trust/DBT India Alliance Senior Fellowship (IA/S/14/1/501307).

References

1. C. R. Cohen, J. Brown, A. B. Moscicki, E. A. Bukusi, J. R. Paull, C. F. Price and S. Shiboski, *PLoS One*, 2011, 6, e16258.
2. I. McGowan, K. Gomez, K. Bruder, I. Febo, B. A. Chen, B. A. Richardson, M. Husnik, E. Livant, C. Price and C. Jacobson, *Aids*, 2011, 25, 1057-1064.
3. D. Sepúlveda-Crespo, R. Gómez, F. J. De La Mata, J. L. Jiménez and M. Á. Muñoz-Fernández, *Nanomedicine: Nanotechnology, Biology and Medicine*, 2015, 11, 1481-1498.
4. R. M. Kannan, E. Nance, S. Kannan and D. A. Tomalia, *J Intern Med*, 2014, 276, 579-617.
5. J. L. Jimenez, M. Pion, F. J. d. l. Mata, R. Gomez, E. Munoz, M. Leal and M. a. A. Munoz-Fernandez, *New Journal of Chemistry*, 2012, 36, 299-309.
6. D. Tyssen, S. A. Henderson, A. Johnson, J. Sterjovski, K. Moore, J. La, M. Zanin, S. Sonza, P. Karellas, M. P. Giannis, G. Krippner, S. Wesselingh, T. McCarthy, P. R. Gorry, P. A. Ramsland, R. Cone, J. R. Paull, G. R. Lewis and G. Tachedjian, *PLoS One*, 2010, 5, e12309.
7. R. Rupp, S. L. Rosenthal and L. R. Stanberry, *Int J Nanomedicine*, 2007, 2, 561-566.
8. C. Mauck, Z. Rosenberg and L. Van Damme, *Aids*, 2001, 15, 857-868.
9. J. W. Romano, M. Robbiani, G. F. Doncel and T. Moench, *Curr HIV Res*, 2012, 10, 9-18.
10. D. C. Chan and P. S. Kim, *Cell*, 1998, 93, 681-684.
11. S. Telwatte, K. Moore, A. Johnson, D. Tyssen, J. Sterjovski, M. Aldunate, P. R. Gorry, P. A. Ramsland, G. R. Lewis, J. R. Paull, S. Sonza and G. Tachedjian, *Antiviral Res*, 2011, 90, 195-199.
12. D. L. Sodora, J. S. Allan, C. Apetrei, J. M. Brenchley, D. C. Douek, J. G. Else, J. D. Estes, B. H. Hahn, V. M. Hirsch, A. Kaur, F. Kirchhoff, M. Muller-Trutwin, I. Pandrea, J. E. Schmitz and G. Silvestri, *Nat Med*, 2009, 15, 861-865.
13. C. Magnus, P. Rusert, S. Bonhoeffer, A. Trkola and R. R. Regoes, *J Virol*, 2009, 83, 1523-1531.
14. S. N. Mulampaka and N. M. Dixit, *PLoS One*, 2011, 6, e19941.
15. V. Maingi, V. Jain, P. V. Bharatam and P. K. Maiti, *J Comput Chem*, 2012, 33, 1997-2011.
16. M. J. Frisch, G. W. Trucks, H. B. Schlegel, G. E. Scuseria, M. A. Robb, J. R. Cheeseman, J. A. Montgomery, T. Vreven, K. N. Kudin, J. C. Burant, J. M. Millam, S. S. Iyengar, J. Tomasi, V. Barone, B. Mennucci, M. Cossi, G. Scalmani, N. Rega, G. A. Petersson, H. Nakatsuji, M. Hada, M. Ehara, K. Toyota, R. Fukuda, J. Hasegawa, M. Ishida, T. Nakajima, Y. Honda, O. Kitao, H. Nakai, M. Klene, X. Li, J. E. Knox, H. P. Hratchian, J. B. Cross, V. Bakken, C. Adamo, J.

Jaramillo, R. Gomperts, R. E. Stratmann, O. Yazyev, A. J. Austin, R. Cammi, C. Pomelli, J. W. Ochterski, P. Y. Ayala, K. Morokuma, G. A. Voth, P. Salvador, J. J. Dannenberg, V. G. Zakrzewski, S. Dapprich, A. D. Daniels, M. C. Strain, O. Farkas, D. K. Malick, A. D. Rabuck, K. Raghavachari, J. B. Foresman, J. V. Ortiz, Q. Cui, A. G. Baboul, S. Clifford, J. Cioslowski, B. B. Stefanov, G. Liu, A. Liashenko, P. Piskorz, I. Komaromi, R. L. Martin, D. J. Fox, T. Keith, A. Laham, C. Y. Peng, A. Nanayakkara, M. Challacombe, P. M. W. Gill, B. Johnson, W. Chen, M. W. Wong, C. Gonzalez and J. A. Pople, 2003.

17. J. Wang, R. M. Wolf, J. W. Caldwell, P. A. Kollman and D. A. Case, *J Comput Chem*, 2004, 25, 1157-1174.
18. D. Case, T. Darden, T. Cheatham III, C. Simmerling, J. Wang, R. Duke, R. Luo, R. Walker, W. Zhang and K. Merz, *There is no corresponding record for this reference*.
19. W. L. Jorgensen, J. Chandrasekhar, J. D. Madura, R. W. Impey and M. L. Klein, *The Journal of Chemical Physics*, 1983, 79, 926-935.
20. J.-P. Ryckaert, G. Ciccotti and H. J. C. Berendsen, *Journal of Computational Physics*, 1977, 23, 327-341.
21. R. Salomon-Ferrer, A. W. Götz, D. Poole, S. Le Grand and R. C. Walker, *Journal of Chemical Theory and Computation*, 2013, 9, 3878-3888.
22. B. Nandy, D. H. Bindu, N. M. Dixit and P. K. Maiti, *J Chem Phys*, 2013, 139, 024905.
23. B. Nandy, M. Santosh and P. K. Maiti, *J Biosci*, 2012, 37, 457-474.
24. C. C. Huang, S. N. Lam, P. Acharya, M. Tang, S. H. Xiang, S. S. Hussan, R. L. Stanfield, J. Robinson, J. Sodroski, I. A. Wilson, R. Wyatt, C. A. Bewley and P. D. Kwong, *Science*, 2007, 317, 1930-1934.
25. A. Pérez, I. Marchán, D. Svozil, J. Sponer, T. E. Cheatham, C. A. Laughton and M. Orozco, *Biophysical Journal*, 2007, 92, 3817-3829.
26. R. Chen, L. Li and Z. Weng, *Proteins*, 2003, 52, 80-87.
27. T. Vreven, B. G. Pierce, H. Hwang and Z. Weng, *Proteins*, 2013, 3, 24432.
28. B. R. Miller, T. D. McGee, J. M. Swails, N. Homeyer, H. Gohlke and A. E. Roitberg, *Journal of Chemical Theory and Computation*, 2012, 8, 3314-3321.
29. D. Kosztin, S. Izrailev and K. Schulten, *Biophys J*, 1999, 76, 188-197.
30. J. C. Phillips, R. Braun, W. Wang, J. Gumbart, E. Tajkhorshid, E. Villa, C. Chipot, R. D. Skeel, L. Kale and K. Schulten, *J Comput Chem*, 2005, 26, 1781-1802.
31. I. Massova and P. Kollman, *Perspectives in Drug Discovery and Design*, 2000, 18, 113-135.
32. D. Sitkoff, K. A. Sharp and B. Honig, *The Journal of Physical Chemistry*, 1994, 98, 1978-1988.
33. B. P. Roberts, M. J. Scanlon, G. Y. Krippner and D. K. Chalmers, *Macromolecules*, 2009, 42, 2775-2783.
34. M. M. Flocco and S. L. Mowbray, *J Mol Biol*, 1994, 235, 709-717.
35. J. B. Mitchell, C. L. Nandi, I. K. McDonald, J. M. Thornton and S. L. Price, *J Mol Biol*, 1994, 239, 315-331.
36. N. Sullivan, Y. Sun, Q. Sattentau, M. Thali, D. Wu, G. Denisova, J. Gershoni, J. Robinson, J. Moore and J. Sodroski, *J Virol*, 1998, 72, 4694-4703.
37. Q. J. Sattentau and J. P. Moore, *J Exp Med*, 1991, 174, 407-415.
38. Q. J. Sattentau, J. P. Moore, F. Vignaux, F. Traincard and P. Poignard, *J Virol*, 1993, 67, 7383-7393.
39. P. Sang, L. Q. Yang, X. L. Ji, Y. X. Fu and S. Q. Liu, *PLoS One*, 2014, 9.
40. D. G. Myszka, R. W. Sweet, P. Hensley, M. Brigham-Burke, P. D. Kwong, W. A. Hendrickson, R. Wyatt, J. Sodroski and M. L. Doyle, *Proc Natl Acad Sci U S A*, 2000, 97, 9026-9031.
41. M. Yokoyama, S. Naganawa, K. Yoshimura, S. Matsushita and H. Sato, *PLoS One*, 2012, 7, 18.
42. R. D. MacArthur and R. M. Novak, *Clin Infect Dis*, 2008, 47, 236-241.

43. M. I. Chang, P. Panorchan, T. M. Dobrowsky, Y. Tseng and D. Wirtz, *J Virol*, 2005, 79, 14748-14755.

Table 1: Energetics of the dendrimer docked to the gp120-CD4 complex. The top 8 structures predicted by ZDOCK were subjected to MD simulations (for >60 ns) and the free energy change associated with the binding of the dendrimer to the gp120-CD4 complex calculated. The docking positions of the various structures are also indicated (snapshots are in Fig. 2).

Rank based on ΔG	ZDOCK rank	Docking position of dendrimer	ΔE (kcal/mol)	TΔS (kcal/mol)	ΔG (kcal/mol)
1	6	Near the V3 loop	-182 ± 10	-111 ± 10	-71 ± 20
2	8	On the V3 loop	-167 ± 11	-100 ± 5	-67 ± 16
3	3	Hanging on the V3 loop and touching the bridging sheet	-169 ± 11	-107 ± 11	-62 ± 22
4	2	On the V3 loop	-146 ± 9	-97 ± 8	-49 ± 17
5	5	On gp120 (near α1 helix)	-108 ± 7	-79 ± 12	-29 ± 16
6	1	Hanging on the V3 loop and touching the bridging sheet	-126 ± 10	-103 ± 9	-23 ± 19
7	7	On gp120	-102 ± 9	-86 ± 2	-16 ± 11
8	4	On gp120	-86 ± 11	-82 ± 18	-4 ± 29

Table 2: Binding energy of gp120 to CD4 in different ternary complexes. The GB binding energy of gp120 to CD4 in the absence or presence of the docked dendrimer computed from the last 30 ns of our equilibrium MD simulations. The 5 complexes in the presence of the dendrimer are indicated by their ranks based on the dendrimer binding free energy listed in Table 1.

Complex	Binding Energy (kcal/mol)
Without dendrimer	-67 ± 7
1	-56 ± 6
2	-68 ± 7
3	-40 ± 7
4	-60 ± 7
8	-47 ± 8

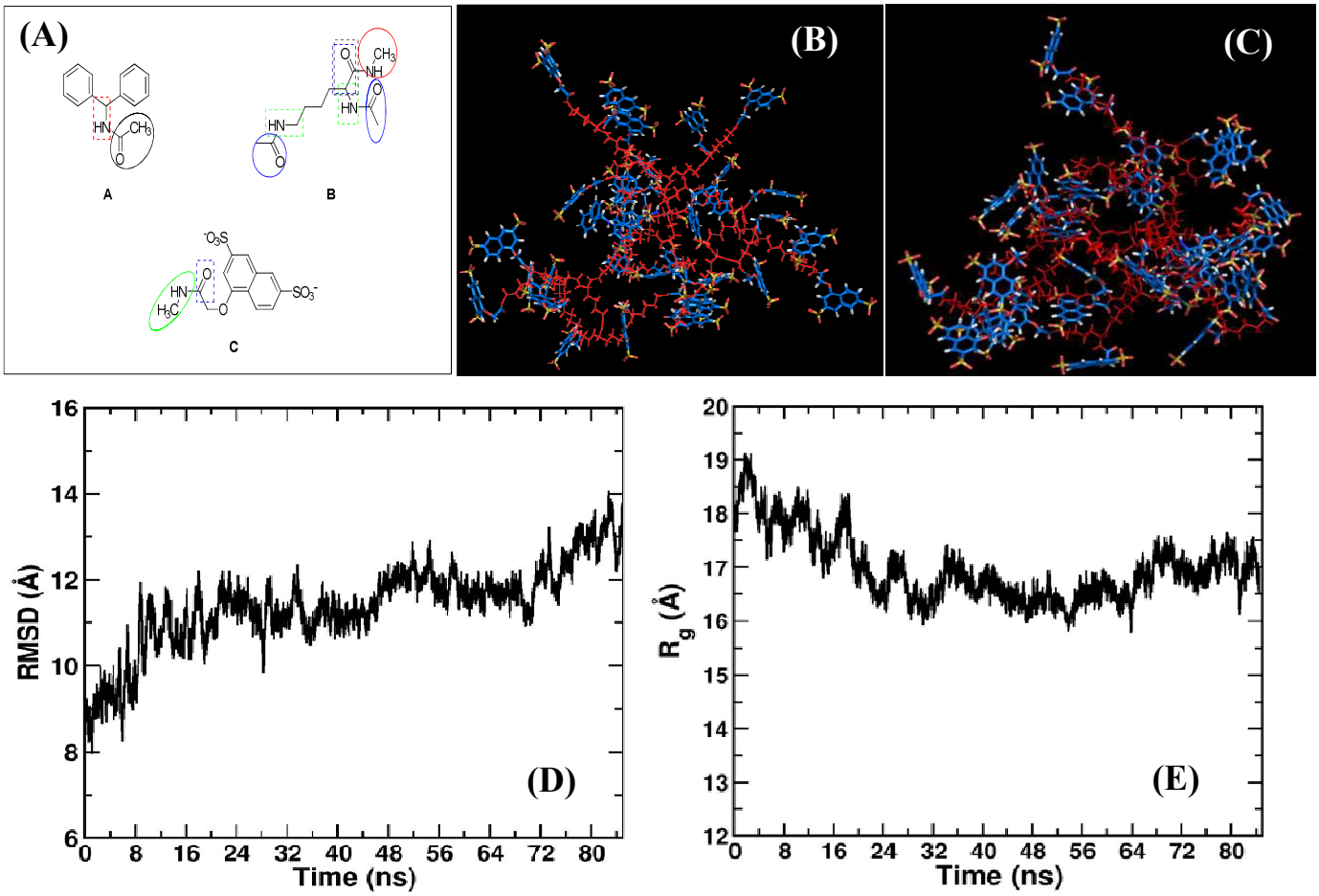

Figure 1. Building of the SPL7013 dendrimer and its equilibration. (A) The three capped residues employed for building the SPL7013 dendrimer: A. the core residue; B. the repeating fragment; C.the terminal residue. During dendrimer building using the dendrimer building toolkit (DBT), the cap regions were identified (ovals or circles) and removed in joining the repeat units. Atoms within the residues (rectangles) identical to those in the cap regions were identified (the identities are color coded). Thus, in connecting the subunits, the cap region of the core, for instance, was removed and the core was then joined to the atoms in the repeating unit that are identical to the removed core. This procedure conserves charges. **(B)** The structure of the generation 4 SPL7013 built using DBT. **(C)** A snapshot of the dendrimer after 52 ns of MD simulation. **(D)** Time-evolution of the RMSD of the dendrimer during the simulation. **(E)** Time-evolution of the radius of gyration of the dendrimer during the simulation.

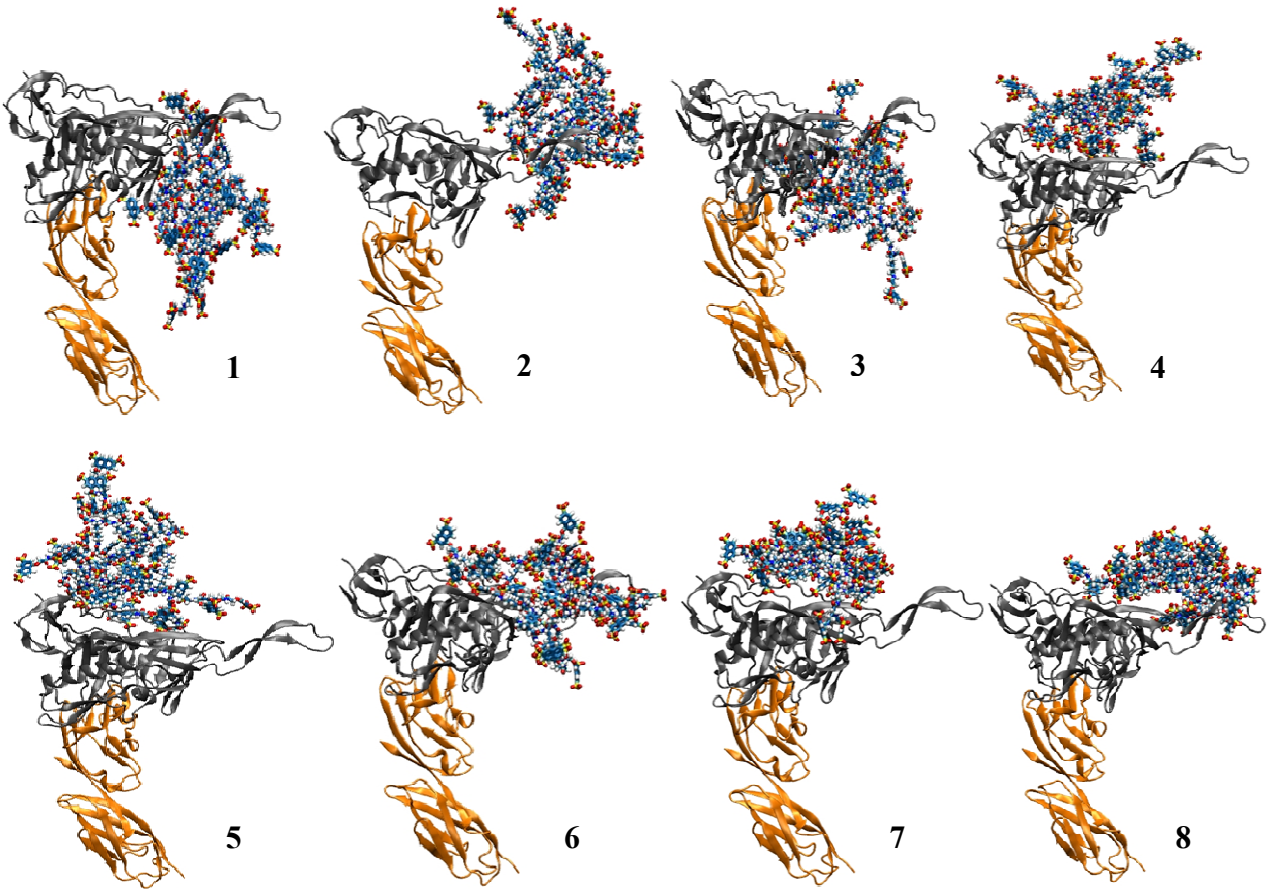

Figure 2. Snapshots of docked structures. Snapshots of the top 8 ranked ZDOCK structures showing the binding position of the SPL7013 dendrimer with respect to the V3 loop. gp120 is shown in gray, CD4 in orange and the SPL7013 dendrimer in blue and orange .

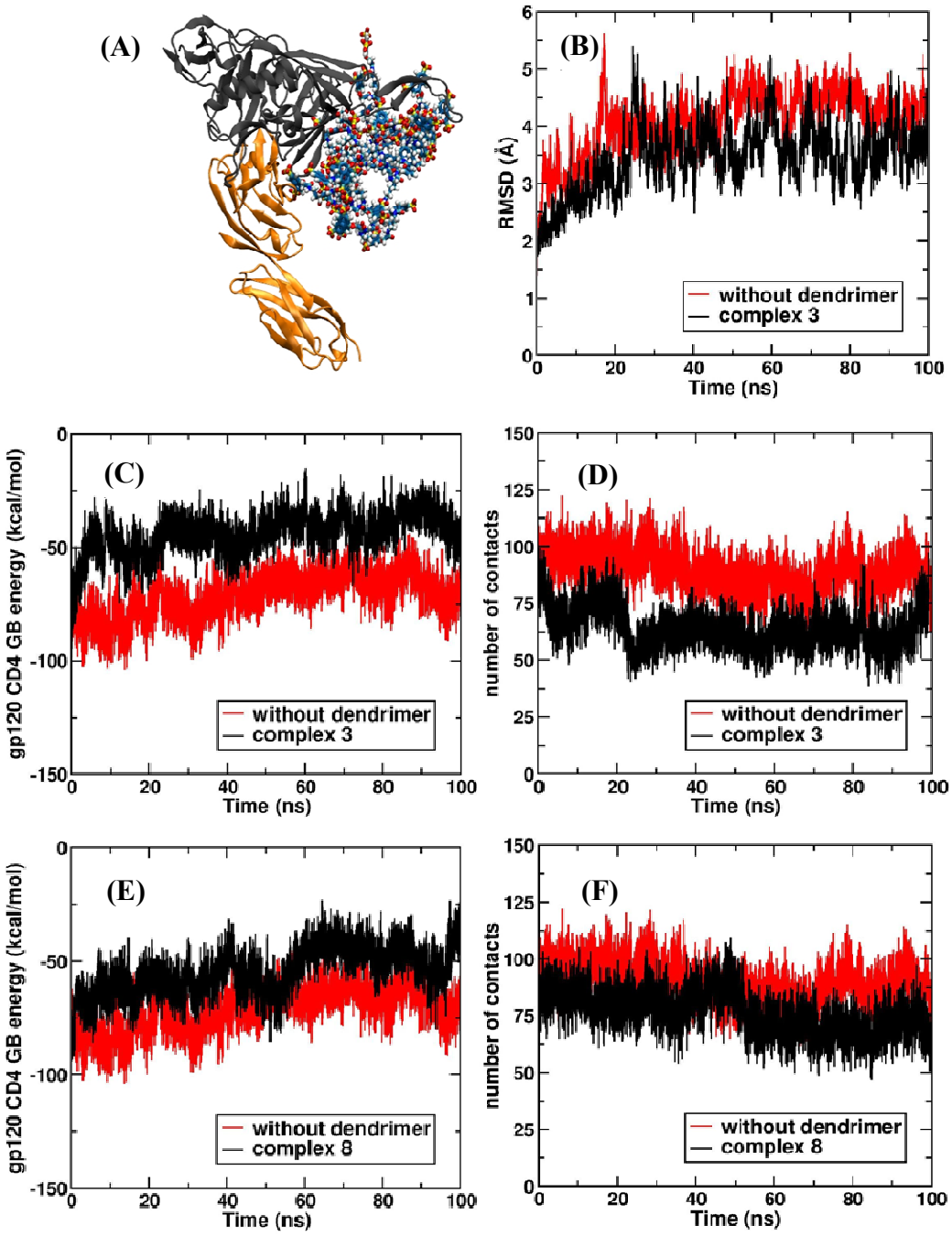

Figure 3. SPL7013 binds to the gp120-CD4 complex and weakens it. (A) A snapshot of the equilibrated structure of complex 3 (see Table 1) showing the binding of SPL7013 (blue and orange) to the gp120 (grey) in the gp120-CD4 complex. (CD4 is in orange.) **(B)** Root mean square deviation (RMSD) of the complex with and without the docked dendrimer. **(C)** GB binding energy and **(D)** the number of contacts between gp120 and CD4 in complex 3 and without the docked dendrimer. **(E)** GB binding energy and **(F)** the number of contacts between gp120 and CD4 in complex 8 and without the docked dendrimer. The corresponding data for the other complexes studied are in Fig. S8.

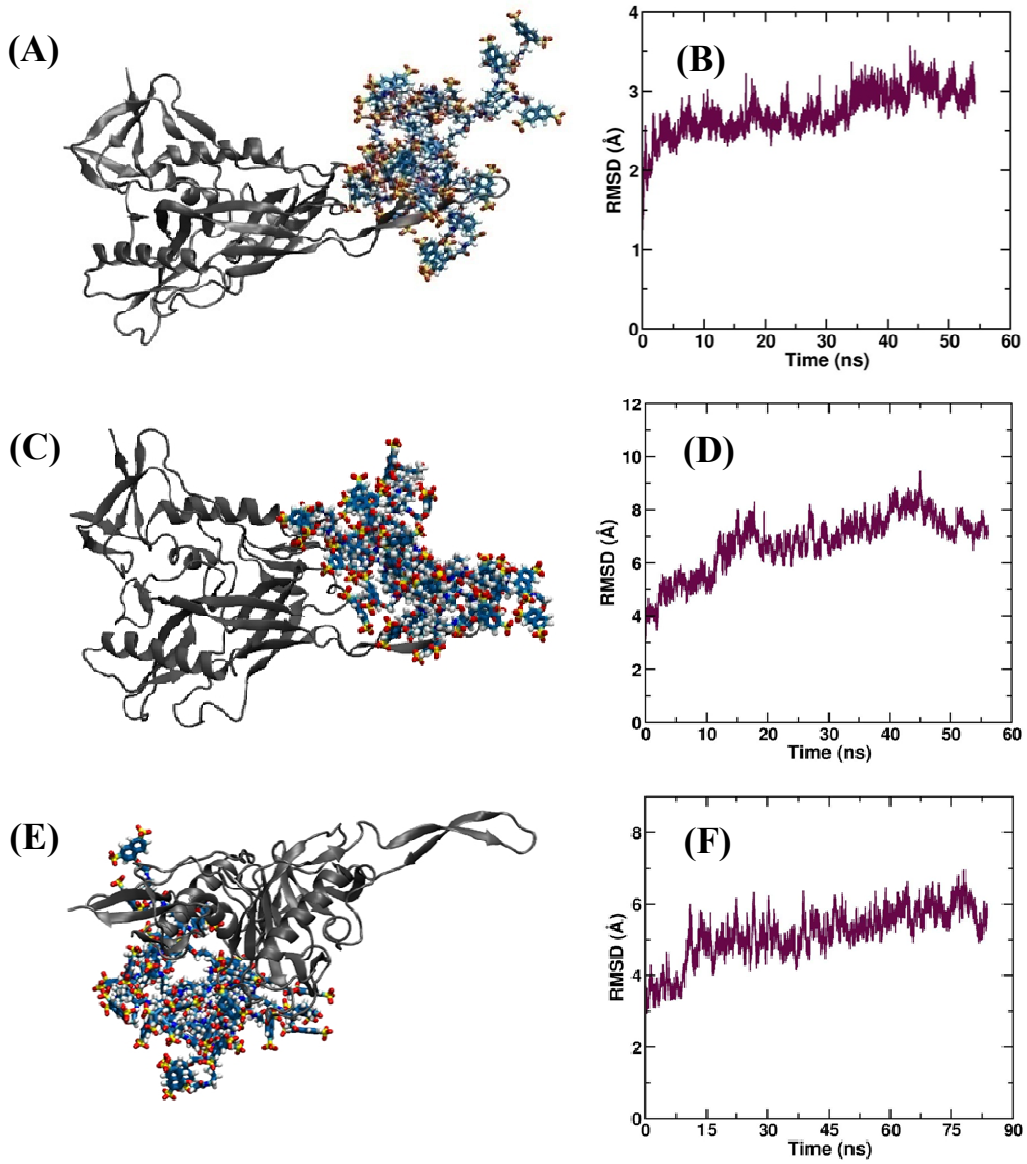

Figure 4. Binding of SPL7013 to gp120 alone. Snapshots of the gp120-SPL7013 complexes predicted by ZDOCK as **(A)** rank 8 and **(C)** rank 1, after equilibration using MD simulations (gp120 is in grey). **(B)** and **(D)** The corresponding root mean square deviations (RMSD) of the complex with respect to their initial configurations. **(E)** A snapshot of the Patchdock structure with the dendrimer blocking the CD4 binding site. **(F)** RMSD of the complex shown in (E) with respect to its initial configuration.

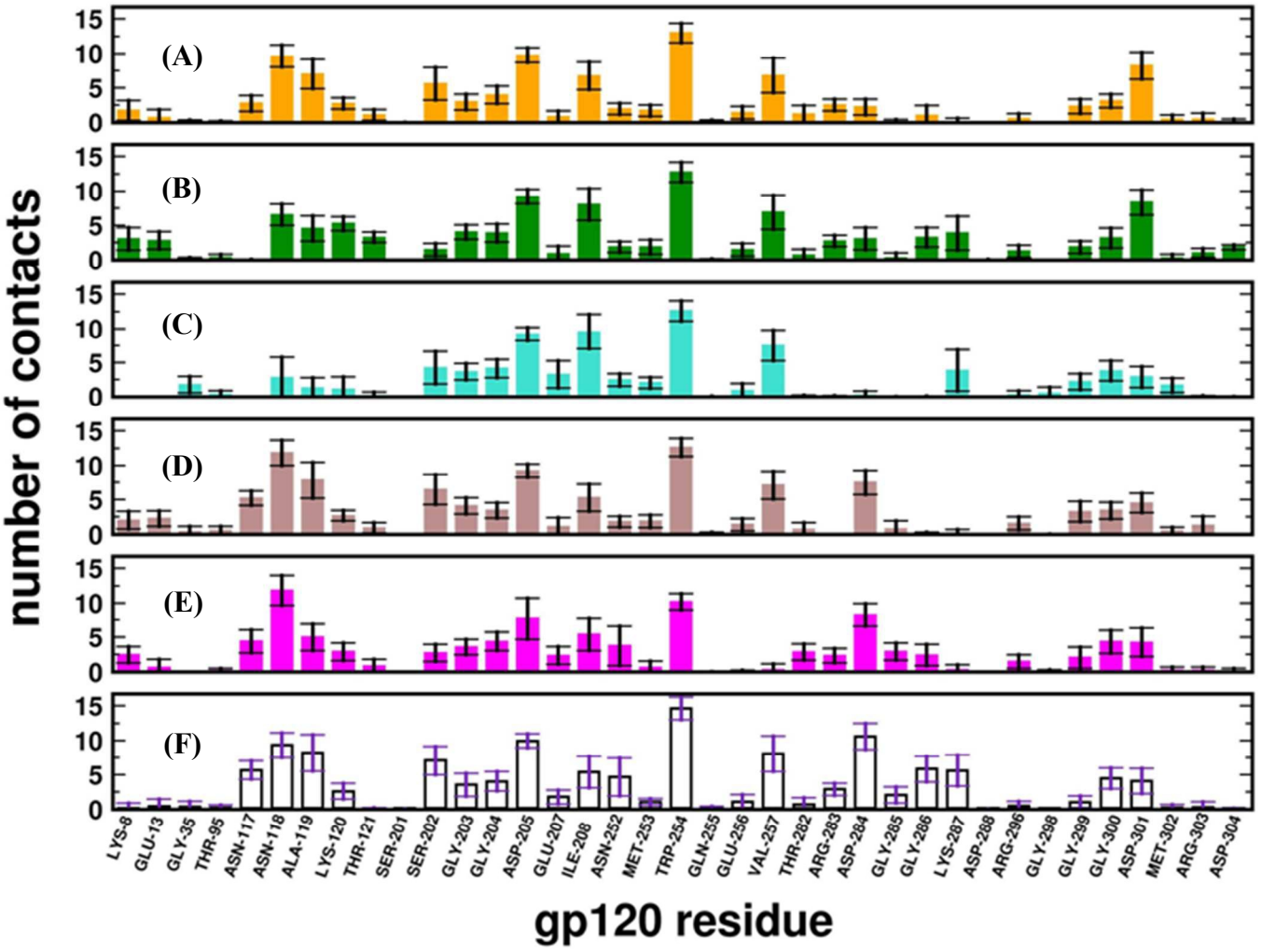

Figure 5: gp120-CD4 contacts with and without the docked dendrimer. The residue-wise contacts of gp120 with CD4 for **(A)** complex 1; **(B)** complex 2; **(C)** complex 3; **(D)** complex 4; **(E)** complex 8; and **(F)** the complex without dendrimer. The mean and error bars are calculated over the last 8 ns of the respective MD trajectories.

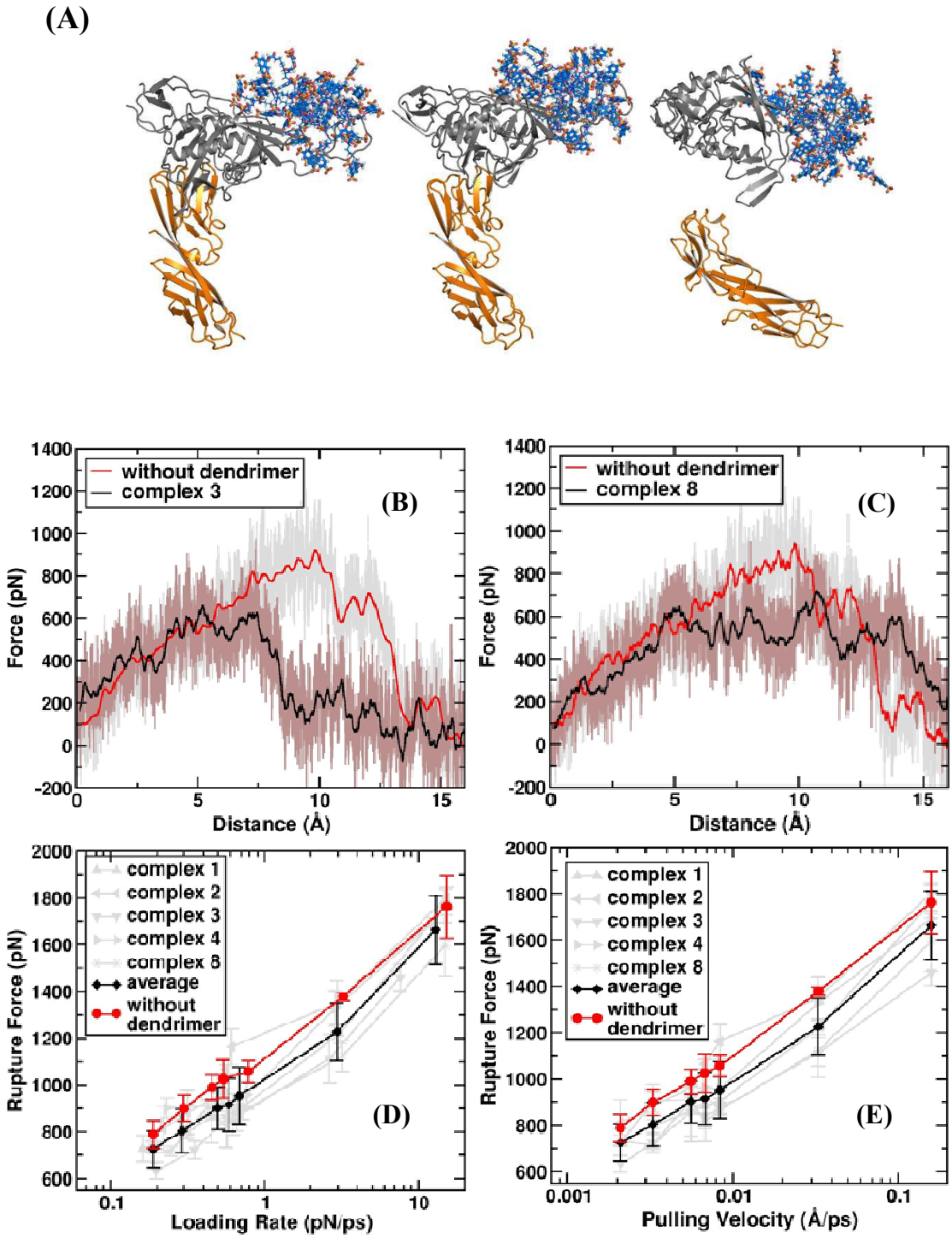

Figure 6. SPL7013 accelerates the dissociation of the gp120-CD4 complex. (A) Snapshots of the gp120-CD4-SPL7013 complex before pulling, at bond rupture, and after complete dissociation, during an SMD simulation. Force versus displacement trajectories during SMD runs with and without dendrimer at a pulling velocity of 0.0021 Å/ps for complex 3 **(B)** and complex 8. The red and black curves are 300-pt. running averages of the gray and brown curves respectively. **(C)**. Average of the rupture force for all the 5 complexes that were selected for pulling, as a function of loading rate **(D)** and pulling velocity **(E)**. The data for the individual complexes are shown in the background and in Fig. S15.

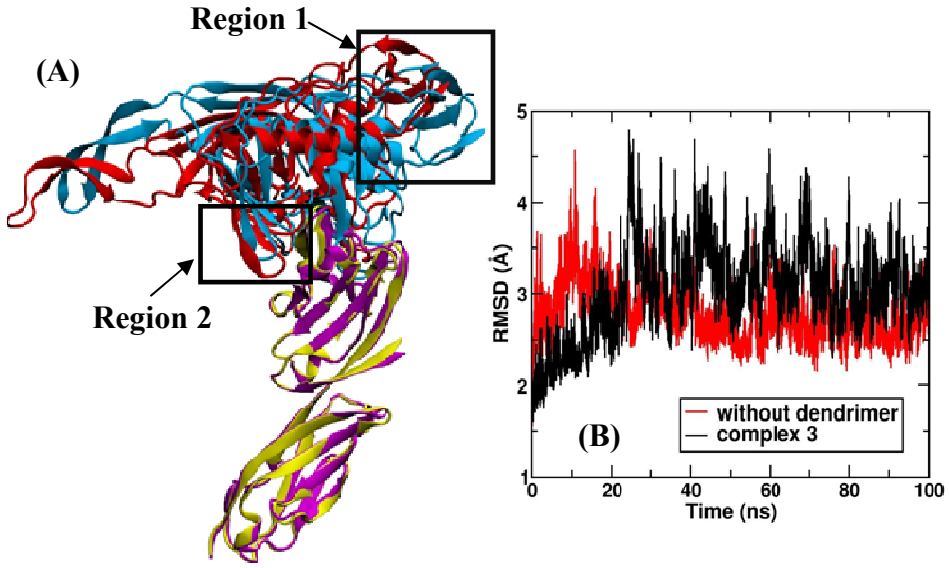

Figure 7: Conformational changes in the gp120-CD4 complex upon dendrimer binding. (A) The structures (gp120 and CD4) corresponding to the average of 400 conformations corresponding to the last 4 ns of MD trajectories of complex 3 (red and yellow) and no dendrimer (blue and mauve) superposed with the CD4 structures aligned. The tilt in gp120 upon dendrimer binding is clearly visible. **(B)** RMSD of the gp120-CD4 complex for the two cases with respect to the corresponding minimized structures, excluding the V3 loop. Complex 3 shows higher RMSD, consistent with the relative tilt.

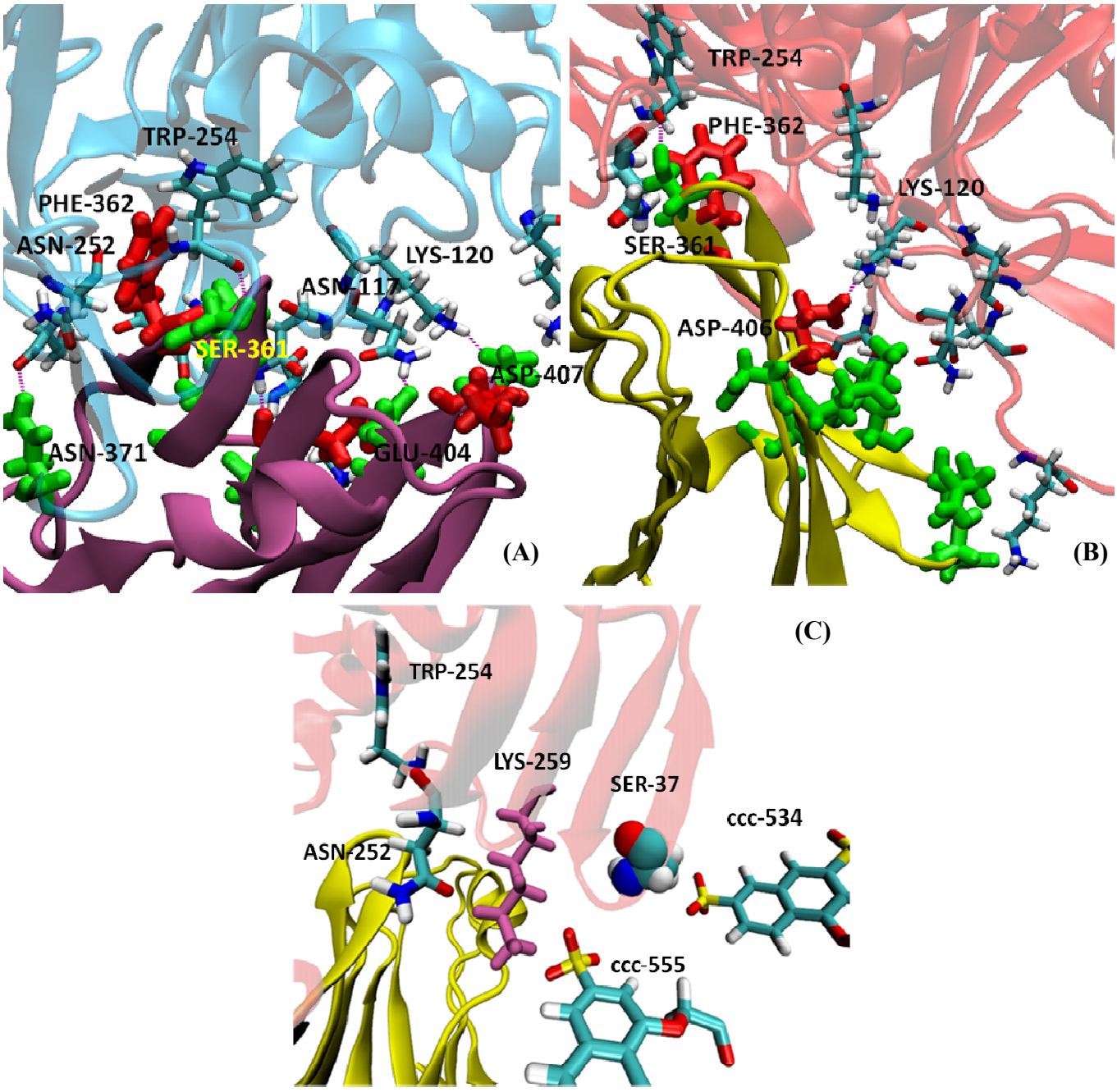

Figure 8: **The protein-dendrimer interface in the presence and the absence of dendrimer**. Hydrogen bonds between the residues of gp120 and CD4 **(A)** without dendrimer and **(B)** for complex 3. Most of the hydrogen bonds are absent in complex 3. The residue pairs forming hydrogen bonds have been labeled. **(C)** Aromatic rings of the SPL dendrimer interacting with the residues of the gp120 bridging sheet in complex 3.